

Thermodynamics of Icing Cylinder for Measurements of Liquid Water Content in Supercooled Clouds

I. P. MAZIN

Central Aerological Observatory, Dolgoprudny, Russia

A. V. KOROLEV

Meteorological Service of Canada, Toronto, Ontario, Canada

A. HEYMSFIELD

National Center for Atmospheric Research, Boulder, Colorado

G. A. ISAAC AND S. G. COBER

Meteorological Service of Canada, Toronto, Ontario, Canada

(Manuscript received 17 March 2000, in final form 14 July 2000)

ABSTRACT

The Rosemount Icing Detector (RICE) has been used extensively over the last three decades for aircraft measurements of the rate of ice riming in supercooled liquid and mixed clouds. Because of difficulties related to calibration and postprocessing, the RICE probe was mainly used as an indicator of the presence of supercooled liquid water. The accuracy of the RICE probe for measurements of supercooled liquid water content is studied here. The theory of ice accretion on an unheated cylinder is applied to the RICE probe. A steady-state heat balance on the surface of a riming cylinder is considered in detail. It is shown that the threshold sensitivity of the RICE probe is limited by the rate of sublimation of ice and it may exceed 0.01 g m^{-3} at airspeed 200 m s^{-1} . The rate of ice sublimation limits the use of the RICE probe for measurements of low liquid water contents in clouds. The maximum possible measured liquid water content is restricted by the Ludlam limit. A new calibration technique of the RICE probe, based on the measurements of the rate of ice sublimation in cloud-free air, is developed here. The calibration coefficient derived using the "sublimation" technique is compared to that obtained using the conventional technique, that is, when ice is accreting on the cylinder. The sublimation technique was found to be more accurate compared to the conventional one. The accuracies of both methods are discussed.

1. Introduction

The Rosemount Icing Detector (RICE) (B.F. Goodrich Rosemount Aerospace Division) is used to detect the rate of ice accretion in supercooled liquid and mixed phase clouds. While it is primarily used on commercial aircraft, during the past three decades a number of research organizations have installed a RICE probe on their research aircraft. The principle of operation of the RICE probe is based on measurements of changes in the natural frequency of a vibrating cylinder due to accretion of ice on its surface. The cylinder is excited by

magnetostrictional forces that cause longitude oscillations of the cylinder at a natural frequency of approximately 40 kHz. It is assumed that liquid supercooled droplets collide and accrete on the surface of the cylinder, whereas solid ice particles bounce off the surface and are swept away with the airflow. Thus ice particles are considered not to affect the measurements. Ice accumulation on the cylinder results in a decrease of the natural frequency of oscillation and the change in frequency F is assumed to be proportional to the mass of the accumulated ice ΔM (Brown 1982), that is, $\Delta F \sim \Delta M$. Variations in the frequency are sensed and converted into a voltage V so that

$$\Delta M = k\Delta V. \quad (1)$$

Techniques for determining the coefficient k have been discussed by Heymsfield and Miloshevich (1989), Baumgardner and Rodi (1989), and Claffey et al. (1995).

Corresponding author address: Alexei Korolev, Cloud Physics Research Division, Meteorological Service of Canada, 4905 Duffering St., Toronto, ON M3H 5T4, Canada.
E-mail: Alexei.Korolev@ec.gc.ca

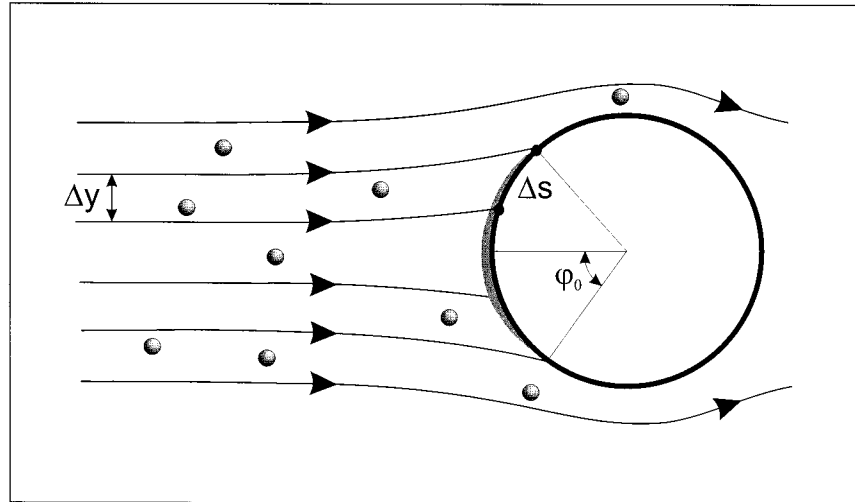


FIG. 1. Scheme of ice growth on a nonrotating cylinder.

The difficulties in defining k are related to simultaneous, accurate measurements of accumulated ice ΔM and frequency changes ΔF . Heymsfield and Miloshevich (1989) suggested calibrating the Rosemount probe by using ΔM derived from Forward Scattering Spectrometer Probe (FSSP) measurements. The limitation of this method is that the FSSP is known to react to ice particles, and it is difficult to determine what fraction of the counts in supercooled clouds were caused by ice and what fraction were caused by liquid droplets. This leads to uncertainty in measurements of ΔM . Baumgardner and Rodi (1989) found that the coefficient k varies from probe to probe, and it depends also on the distribution of ice over the cylinder surface. They obtained a different k coefficient than that reported by Heymsfield and Miloshevich (1989). Claffey et al. (1995) calibrated three RICE probes using a rotating multicylinder at the Mt. Washington Observatory. They found that each ice detector was unique and should be calibrated individually before being used.

This paper presents a theoretical study of ice accretion on the surface of the cylinder in the flow of supercooled droplets. A steady-state heat balance on the surface of the icing cylinder is considered in detail. A new calibration technique for the RICE probe, based on the measurements of the rate of ice sublimation in cloud-free air, is suggested. The calibration coefficient derived using this sublimation technique is compared with that obtained using the conventional technique, that is, when ice is accreting on the cylinder.

2. Heat balance on the surface of a riming cylinder

Consider a cylinder exposed to the flow of air with velocity U , temperature T_a , pressure P_a , and containing supercooled droplets with radius r and liquid water con-

tent (LWC) W . It is assumed that the axis of the cylinder is perpendicular to the axis of the vector of the air velocity. The temperature of the droplets is considered to be the same as the temperature of the air. In the vicinity of the cylinder the trajectories of the droplets due to their inertia will deviate from the trajectories of the air. As a result the droplets will hit the cylinder within a certain band limited by polar angles $-\varphi_0$ to φ_0 (Fig. 1). The angle φ_0 is a function of the droplet radius, cylinder radius, airspeed, air temperature, and pressure (Langmuir and Blodgett 1945; Mazin 1957; Borovikov et al. 1963). At angles $\varphi > |\varphi_0|$ the droplets with radii r do not impact the cylinder and they flow around the cylinder with the airflow. Thus in the case of supercooled droplets, ice would accrete on the surface of the cylinder where $\varphi < |\varphi_0|$. In principle, the shape of the accreted ice depends on the airspeed, droplet size, LWC air temperature, and other parameters that define the thermodynamical processes on the icing surface. The shape of the accreted ice is also a function of time and can vary significantly from that shown in Fig. 1.

The shape of accreted ice on a cylindrical surface has been discussed in a number of studies (e.g., Mazin 1957; Lozowski et al. 1983a,b). The RICE probe automatically de-ices itself with an internal heater after approximately 0.5 mm of ice accumulates on its surface. This value is small compared to the RICE cylinder diameter (≈ 6.3 mm). Therefore, in this study it is assumed that the ice accreted on the RICE probe surface has a shape close to that of a circular cylinder. The spongy ice formation and runback icing is not considered in the frame of this study.

a. Local heat balance

The pioneering work on heat balance of an icing surface goes back to the 1950s (e.g., Hardy 1945; Ludlam

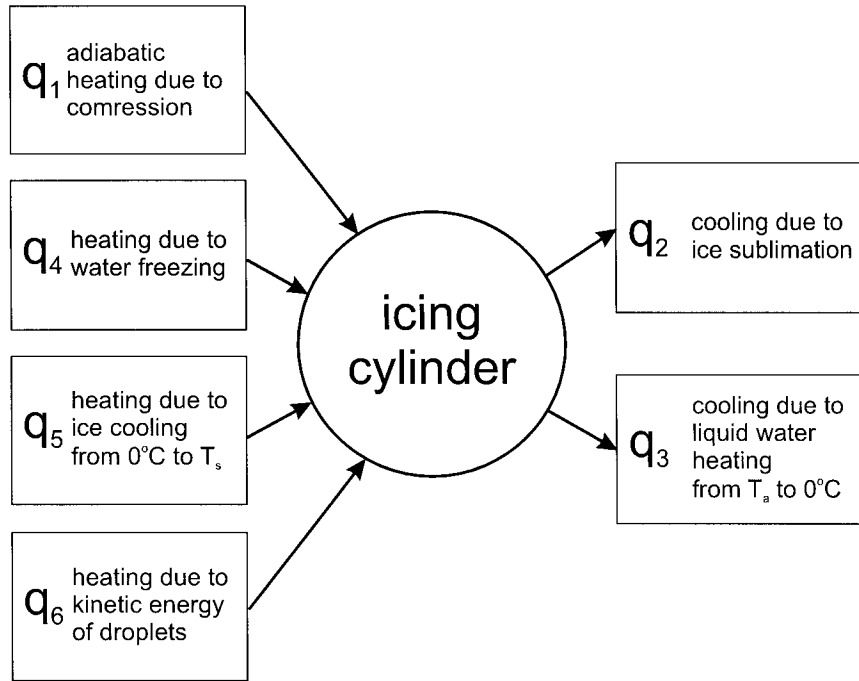


FIG. 2. Scheme of the heat fluxes to the circular icing cylinder (see text).

1951; Tribus 1951; Messinger 1953; Fraser et al. 1953; Hardy and Brown 1954). A detailed discussion of these papers can be found in Mazin (1957).

Consider a steady-state heat balance at a local point on the surface of the cylinder. The surface temperature is defined by several processes: dynamic heating, freezing of droplets, ice sublimation, heat exchange between the droplets, and the cylinder's surface. These processes are schematically shown in Fig. 2. Due to axial symmetry of the cylinder, the thermal processes on the surface will be a function of the polar angle φ (Fig. 1).

The equation of the heat balance at a local point can be written as

$$\sum q_i = 0, \quad (2)$$

where q_i are the densities of the heat fluxes resulting from different processes. The value of q_i is defined as an amount of heat passing through the unit surface per unit time ($\text{J m}^{-2} \text{s}^{-1}$). Because of dynamic heating and latent heat release from freezing droplets, the surface temperature of the cylinder will normally be higher than the ambient temperature.

The heat flux q_1 is related to the aerodynamic heating due to adiabatic compression of the air. In the following discussion the thermal conductivity of ice is neglected, resulting in no heat flux inside the cylinder. In this case the adiabatic temperature on the cylinder's surface is (e.g., Hilton 1951):

$$T_{sA} = T_a + \frac{\kappa U^2}{C_p}, \quad (3)$$

where C_p is the specific heat capacity of the air at constant pressure, and κ is the recovery factor. The factor κ takes into account the dissipation of energy due to internal friction. For air the value of the recovery factor can be assumed to be $\kappa \approx \sqrt{\text{Pr}}$ (e.g., Incropera and DeWitt 1985), where Pr is the Prandtl number. For air, $\text{Pr} \approx 0.72$ and $\kappa \approx 0.85$. Experimental measurements have shown that the recovery factor varies along the surface of the cylinder from 1 to 0.5 (Seban 1960; Lozowski et al. 1983a).

Because of droplet freezing, ice evaporation, and other thermal processes (Fig. 2), the surface temperature $T_{s\varphi}$ may be different from the adiabatic one, that is, $T_{s\varphi} \neq T_{s\varphi A}$. The convective heat losses at the cylinder's surface, defined by a polar angle φ , can be presented as

$$q_1 = -\alpha_\varphi(T_{s\varphi} - T_{s\varphi A}), \quad (4)$$

where α_φ is the heat transfer coefficient that describes the amount of heat per unit temperature interval that comes to the unit of surface area during a unit time interval (e.g., Incropera and DeWitt 1985). The coefficient α_φ varies along the surface of the cylinder (appendix A). The flux q_1 is considered to be positive if the heat is directed toward the cylinder surface from outside; that is, if $T_{s\varphi A} > T_{s\varphi}$.

If the cylinder surface is covered with ice and the vapor pressure of the air e_a is less than its saturated value with respect to ice $E_{i\varphi}$ at the surface temperature $T_{s\varphi}$, then the heat flux q_2 associated with ice evaporation is

$$q_2 = -m_{i\varphi} L_{i\varphi}, \quad (5)$$

where $L_{i\varphi}$ is the latent heat of sublimation at temperature $T_{s\varphi}$, and $m_{i\varphi}$ is the mass of the ice sublimated from the unit surface area during the unit time. Assuming that the water vapor is saturated with respect to ice $E_{i\varphi}$ at the ice surface (Mazin 1957):

$$m_{i\varphi} = b \frac{\alpha_\varphi (\rho_{vs} - \rho_{va})}{C_p \rho_a}. \quad (6)$$

Here ρ_{vs} , ρ_{va} are the densities of the saturated water vapor at surface and air temperatures, respectively, and ρ_a is the air density. Minervin (1956) showed that the coefficient b deviates from unity by not more than about 1%. Lozowski et al. (1983a) used $b = (\text{Pr}/\text{Sc})^{0.63}$, where Pr and Sc are the Prandtl and Schmidt numbers, respectively. This coefficient is rather close to unity as well [at $T_a = -10^\circ\text{C}$, $(\text{Pr}/\text{Sc})^{0.63} = 1.13$]. In the following consideration it is assumed that $b = 1$ and it is omitted in the equations.

After substituting ρ_{vs} , ρ_{va} , ρ_a , Eq. (6) may be rewritten as

$$m_{i\varphi} = \frac{\alpha_\varphi R_a (E_{i\varphi} - e_a)}{C_p R_v P_a \left(1 - \frac{E_{i\varphi}}{P_a}\right) \left(1 - \frac{e_a}{P_a}\right)} \approx \frac{\alpha_\varphi R_a (E_{i\varphi} - e_a)}{C_p R_v P_a}. \quad (7)$$

Substituting Eq. (7) in Eq. (5) yields

$$q_2 = -\frac{\alpha_\varphi R_a L_{i\varphi} (E_{i\varphi} - e_a)}{C_p R_v P_a}, \quad (8)$$

where R_a and R_v are the specific gas constants of air and water vapor, respectively, and P_a is the air pressure. The flux q_2 is directed outward from the cylinder surface if ice evaporates, that is, when $E_{i\varphi} > e_a$. Equations (3) and (8) show that the rate and the sign of ice mass changes on the cylinder surface depend on the air temperature T_a , surface temperature T_s , water vapor pressure e_a , and airflow velocity U .

The process of ice accretion on the cylinder surface can be divided into three steps. During the first step, supercooled water accreted on the surface of the cylinder is heated from temperature T_a to 0°C following:

$$q_3 = m_{w\varphi} C_w (T_a - 0) = m_{w\varphi} C_w T_a. \quad (9)$$

In the second step, the water freezes at temperature 0°C , and the corresponding heat flux is

$$q_4 = m_{w\varphi} L_f. \quad (10)$$

Finally the frozen water cools from 0°C down to the surface temperature $T_{s\varphi}$ following

$$q_5 = m_{w\varphi} C_i (0 - T_{s\varphi}) = -m_{w\varphi} C_i T_{s\varphi}. \quad (11)$$

Here C_w and C_i are the specific thermal capacity of water and ice, respectively; L_f is the specific latent heat of water freezing at temperature 0°C ; and $m_{w\varphi}$ is the mass flux of the supercooled water deposited on a unit surface of the cylinder surface during a unit time ($\text{kg m}^{-2} \text{s}^{-1}$).

The heat flux q_3 is negative, while the fluxes q_4 and q_5 are positive.

The term $m_{w\varphi}$ is associated with the flow of droplets, and can be presented as

$$m_{w\varphi} = \varepsilon_\varphi U W \cos\varphi, \quad (12)$$

where W is the liquid water content; $\varepsilon_\varphi = \varepsilon_\varphi(\varphi, \text{Stk}, \text{Re})$ is the local collision efficiency; $\text{Stk} = (2Ur^2)/(9\mu R_c)$ ρ_w is the Stokes number; $\text{Re} = (2Ur)/\nu$ is the Reynolds number for droplets of radius r ; R_c is the radius of cylinder; μ and ν are the dynamic and kinematic viscosity of the air, respectively; and ρ_w is the water density. The product $\varepsilon_\varphi \cos\varphi$ is the ratio of the distance Δy between the neighboring trajectories of droplets of radius r far away from the cylinder to the length of the arc Δs resulting from the intersection of the trajectories and the cylinder (Fig. 1). In case of a polydisperse droplet size distribution $n(r)$ the local collision efficiency should be replaced by the integral one

$$\varepsilon_{\varphi 0} = \frac{\int_0^\infty \varepsilon_\varphi(r) r^3 n(r) dr}{\int_0^\infty r^3 n(r) dr}. \quad (13)$$

A heat flux related to the kinetic energy of droplets hitting the cylinder is

$$q_6 = \frac{m_{w\varphi} U^2}{2}. \quad (14)$$

The fluxes q_1 and q_2 make the major contribution to the equation of heat balance Eq. (2), while the flux q_6 is about one–two orders magnitude smaller compared to other terms in Eq. (2). Therefore, the term q_6 is neglected. The radiation flux is also neglected and it is assumed that there is no heat transfer along the surface of the cylinder (Lozowski and d'Amours 1980; Makkonen 1981). Combining Eqs. (2)–(4) and Eqs. (8)–(12) gives an equation for the steady-state heat balance:

$$\alpha_\varphi \left(T_a - T_{s\varphi} + \frac{\kappa U^2}{2C_p} - \frac{R_a L_{i\varphi}}{C_p R_v P_a} (E_{i\varphi} - e_a) \right) + \varepsilon_{\varphi 0} U W \cos\varphi (L_f - C_i T_{s\varphi} + C_w T_a) = 0. \quad (15)$$

Equation (15) describes the heat balance at a local point on the surface of the cylinder. The RICE probe response depends on the mass of accreted ice and its distribution on the surface of the cylinder (Baumgardner and Rodi 1989). In the following discussion it is assumed that ice is distributed uniformly along the axis of the cylinder.

b. Integral heat balance

In practice, the use of Eq. (15) is limited since it describes the heat balance at a local point. This problem can be solved by considering the heat balance over the

whole ice surface. For this Eq. (15) is integrated over the cylinder surface covered by ice as

$$\frac{\kappa U^2}{2C_p} + T_a - T_s - \frac{R_a L_i}{C_p R_v P_a} (E_i - e_a) + \frac{\varepsilon U W}{\varphi_0 \xi \alpha} (L_f - C_i T_s + C_w T_a) = 0. \quad (16)$$

Here T_s is the temperature averaged over the surface covered by ice, that is, over the sector limited by the angles $-\varphi_0$ to φ_0 ; $L_i = L_i(T_s)$ is the latent heat of evaporation at temperature T_s ; $E_i = E_i(T_s)$ is water vapor pressure saturated over ice at temperature T_s , $\varepsilon = \int \varepsilon_\varphi \cos \varphi d\varphi$ is the integral collision efficiency (appendix B), $\overline{\alpha_\varphi} = \xi \alpha$ is the heat transfer coefficient for a cylinder averaged over the angle range $-\varphi_0$ to φ_0 , α is the heat transfer coefficient averaged over the whole cylinder, that is, $-\pi < \varphi_0 < \pi$ (appendix A); ξ is a coefficient defined by the angle φ_0 (appendix A).

For Eq. (16), the following assumptions were made:

$$\overline{\alpha_\varphi (T_a - T_{s\varphi})} \approx \xi \alpha (T_a - T_s), \quad (17)$$

$$\overline{\alpha_\varphi L_{i\varphi} (E_{i\varphi} - e_a)} \approx \xi \alpha L_i (E_i - e_a). \quad (18)$$

These assumptions work with a reasonable accuracy, if changes of the variables along the surface are relatively small. Estimates show that if $U < 180 \text{ m s}^{-1}$ α_φ and T_s change by not more than $\pm 30\%$. The averaged product of the above variables deviate from the product of the averaged ones by no more than 10%–15%.

3. Threshold liquid water content

In this section, a liquid water content W_{e0} is derived, which balances the ice sublimation. The mass of sublimating ice per unit time M_e can be found by integrating Eq. (7) over the icing surface as

$$M_{e0} = \frac{2R_c l \xi \alpha \varphi_0 R_a}{C_p R_v P_a} (E_i - e_a). \quad (19)$$

Here l is the length of icing cylinder. The liquid water content, which balances the sublimating ice, M_{e0} , is

$$W_{e0} = \frac{M_e}{2R_c l \varepsilon U} = \frac{\varphi_0 \alpha \xi}{\varepsilon U} \frac{R_a}{C_p R_v P_a} (E_i - e_a). \quad (20)$$

To calculate W_{e0} from Eq. (20) we require E_i , which is a function of T_s . To find T_s , substitute Eq. (20) in Eq. (16) and take into account that $L_i + C_i T_s = L_{i0}(0^\circ\text{C})$ to obtain

$$\frac{\kappa U^2}{2c_p} + T_a - T_s - \frac{R_a}{C_p R_v P_a} (E_i - e_a) (L_{i0} - L_f - C_w T_a) = 0. \quad (21)$$

Equation (21) contains only one unknown variable T_s , which can be computed using numerical methods.

Figure 3 shows the dependence of the difference T_s

– T_a versus the air velocity U for different: (a) air temperatures T_a , (b) relative humidity e_a/E_w , and (c) air pressure P_a . As is seen from Fig. 3, the ice sublimation results in additional cooling of the surface compared to a dry cylinder (curve $T_s = T_{sA}$). The effect of cooling depends on T_a , e_a/E_w , P_a , and U , and it increases with an increase of the air temperature (Fig. 3a), a decrease of relative humidity (Fig. 3b), and a decrease of pressure (Fig. 3c). At $U = 100 \text{ m s}^{-1}$ the effect of cooling is about 2°C (Fig. 3a at $T_a = -5^\circ\text{C}$, $P_a = 800 \text{ mb}$), while at $U = 200 \text{ m s}^{-1}$ the effect increases up to 9°C (Fig. 3c at $T_a = -10^\circ\text{C}$, $P_a = 400 \text{ mb}$). At low temperatures ($T_a < -40^\circ\text{C}$) the cooling effect becomes insignificant (Fig. 3a). Under certain conditions [i.e., when $e_a > E_i(T_s)$] the effect of ice sublimation may exceed the adiabatic heating and the temperature of the surface of the ice becomes lower than the temperature of the air (Fig. 3b). Such situations may occur if the air is dry. This phenomenon is similar to the cooling of a wet thermometer. The analysis of Eq. (21) shows that under certain conditions the deposition of ice on the surface of the cylinder from water vapor is possible. It is worth noting that T_s in Eq. (22) does not depend on the collection efficiency ε and the angle φ_0 .

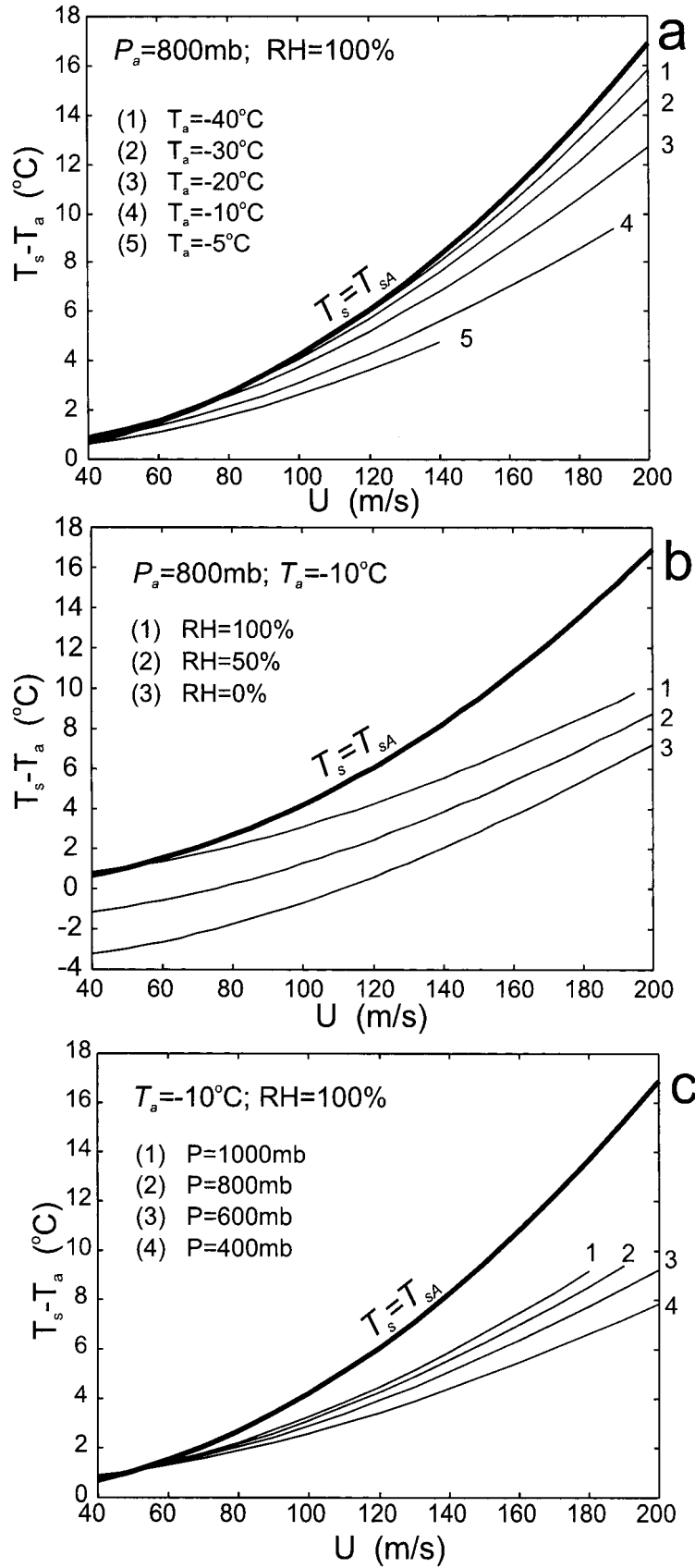
Figure 4 shows the dependence of W_{e0} on airspeed using Eq. (20), for different air pressures and humidity. Though the zero relative humidity case is unrealistic for in-cloud regions, the examples of W_{e0} calculated for zero humidity give an idea about the behavior of W_{e0} . This may be useful for studies of icing in wind tunnels or simulated icing behind air tankers where the humidity may be significantly less 100%. For calculations of W_{e0} the radius of the droplets was assumed to be $r = 10 \mu\text{m}$ and the collision efficiency ε , angle φ_0 , and coefficient ξ were calculated based on this droplet size (appendixes A and B).

It is seen from Fig. 4 that W_{e0} increases with increasing temperature and airspeed in saturated air. The characteristic values of W_{e0} in saturated air at $U = 100 \text{ m s}^{-1}$ is of the order of 0.005 g m^{-3} . At $U = 200 \text{ m s}^{-1}$ W_{e0} exceeds 0.01 g m^{-3} at $T_a > -20^\circ\text{C}$.

The value W_{e0} is an important parameter, since it defines a theoretical lower threshold for liquid water content measurements by the RICE probe; that is, the RICE probe cannot measure liquid water content less than W_{e0} . If $W = W_{e0}$ the RICE probe will measure zero LWC, and if $W < W_{e0}$ the RICE signal will decrease, if it was not zero. Another important conclusion is that it is necessary to make corrections for the mass of sublimating ice when the LWC is of the order of 0.01 g m^{-3} , and it becomes comparable with the amount of sublimating ice. This is important for aircraft with speeds higher than 150 m s^{-1} .

4. Saturated liquid water content (Ludlam limit)

An increase of the LWC leads to an increase of the heat flux q_4 . At some LWC the heat of freezing will



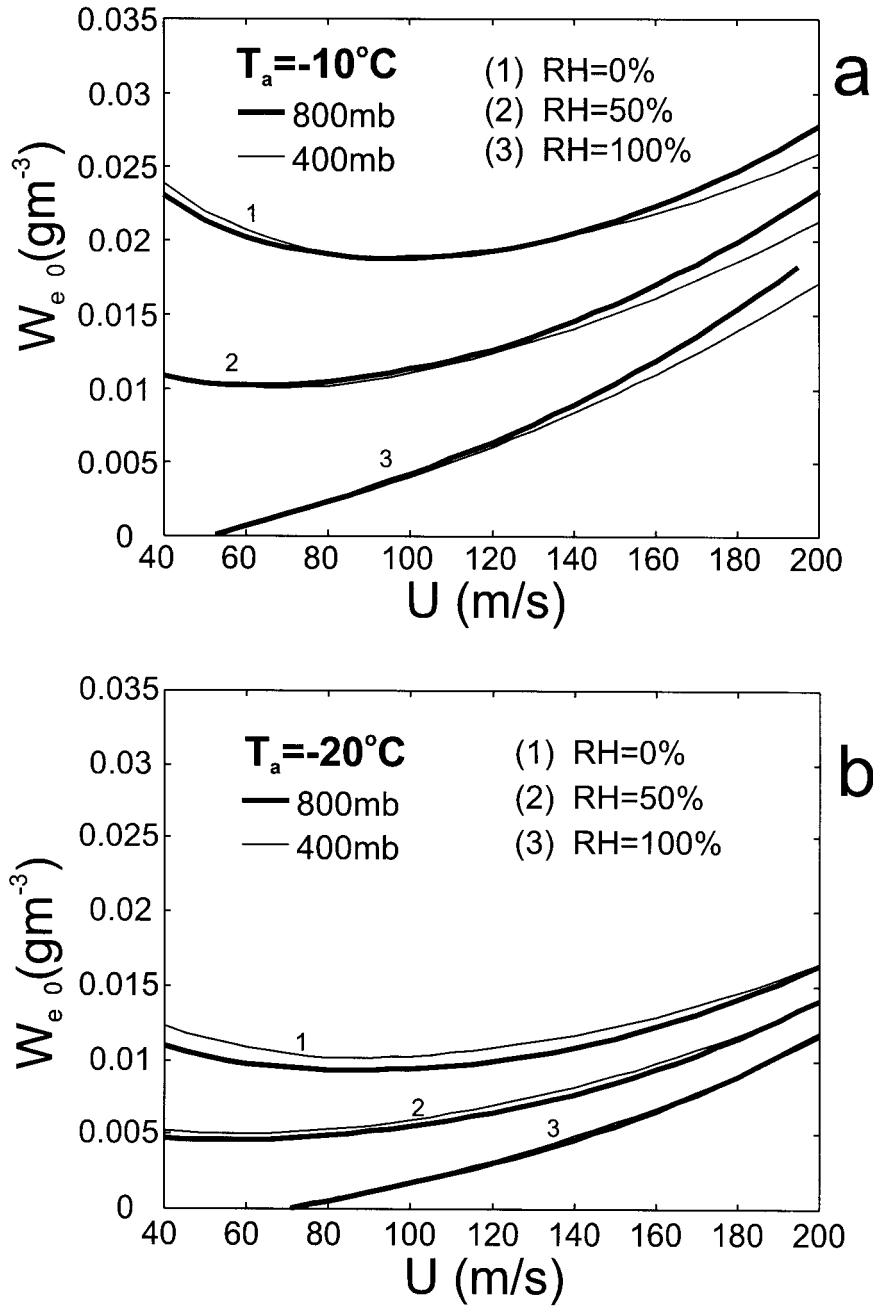


FIG. 4. Liquid water content W_{e0} that compensates the ice sublimation from the surface of RICE probe cylinder vs airspeed U at different pressure P_a , temperature T_a , and relative humidity RH.

←

FIG. 3. Deviation of the ice surface temperature from the adiabatic value $\Delta T_s = T_s - T_a$ vs airspeed U at different pressure P_a , air temperature T_a , and relative humidity RH in the atmosphere with respect to water. The calculations were made for the cylinder having RICE probe radius 3.15 mm.

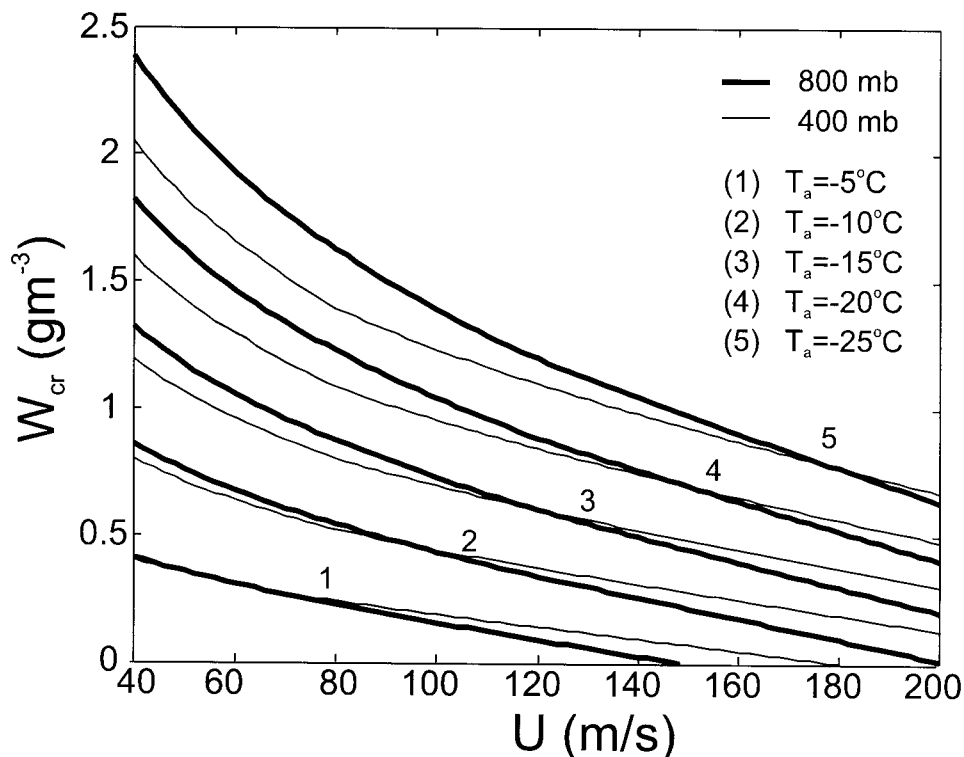


FIG. 5. The Ludlam limit W_{cr} (critical LWC at which the surface temperature rises to 0°C) vs airspeed U for different pressure P_a , temperature T_a .

increase the surface temperature T_s to 0°C . Further increase in the LWC will not result in an increase in the surface temperature. In this case only a fraction of the supercooled water freezes. This fact may be taken into account by introducing the coefficient of freezing (Mazin 1957; Borovikov et al. 1963). The minimum value of the LWC $W = W_{cr}$ at which T_s reaches 0°C is called the Ludlam limit (Ludlam 1951). The unfrozen fraction of liquid water may shed away with the airflow or freeze at the backside of the cylinder (runback icing), or may be partly incorporated into a spongy ice structure similar to hail growth (Greenan and List 1995). For the RICE probe an increase in the LWC above W_{cr} would cause a dropoff of the rate of change of the output signal, so that for LWCs $W > W_{cr}$ cannot be accurately measured by the RICE probe. Baumgardner and Rodi (1989) and Cober et al. (2001) demonstrated this effect in RICE measurements when the Ludlam limit is reached. Thus, W_{cr} can be considered as an upper limit of supercooled LWC that can be measured by RICE probe.

The value of W_{cr} can be derived from Eq. (16), assuming $T_s = 0^{\circ}\text{C}$ and that the vapor pressure is equal to the saturated value with respect to water $e_a = E_w(T_a)$:

$$W_{cr} = \frac{\frac{\xi R_a L_{is}}{\varepsilon U} C_p R_v P_a [E_w(0) - E_w(T_a)] - \frac{\kappa U^2}{2c_p} - T_a}{L_f + C_w T_a}. \quad (22)$$

The results of W_{cr} calculations are presented in Fig. 5. As seen in Fig. 5, W_{cr} increases rapidly with decreasing T_a and an increasing U . At temperatures $T_a > -10^{\circ}\text{C}$ and $U > 100 \text{ m s}^{-1}$ the situation when $W > W_{cr}$ is quite typical for clouds and the Ludlam limit may be easily reached.

5. Calculation of T_s , W_e , W

Consider the process of ice deposition on the surface of the RICE probe cylinder. Assume M is the total mass of droplets that impact the surface of the cylinder and freeze during the time period Δt . Some part of the ice M_e will sublimate and another part M_a will stay on the cylinder as accreted ice. The mass balance on the surface yields

$$M\Delta t = (M_a + M_e)\Delta t = 2R_c l \varepsilon U (W_a + W_e)\Delta t, \quad (23)$$

where W_a and W_e are the fractions of LWCs that accrete as ice on the cylinder and sublimate, respectively. Since only M_a causes the RICE probe response, Eq. (23) using Eq. (1) can be rewritten as

$$W = W_a + W_e = \frac{k}{2R_c l \varepsilon U} \frac{\Delta V}{\Delta t} + W_e. \quad (24)$$

The values of T_s , W_e , and W can be found iteratively using Eqs. (16) and (20). For calculation of W and T_s at $U = 175 \text{ m s}^{-1}$, $P_a = 400 \text{ mb}$, $T_a = -20^{\circ}\text{C}$, and W_m

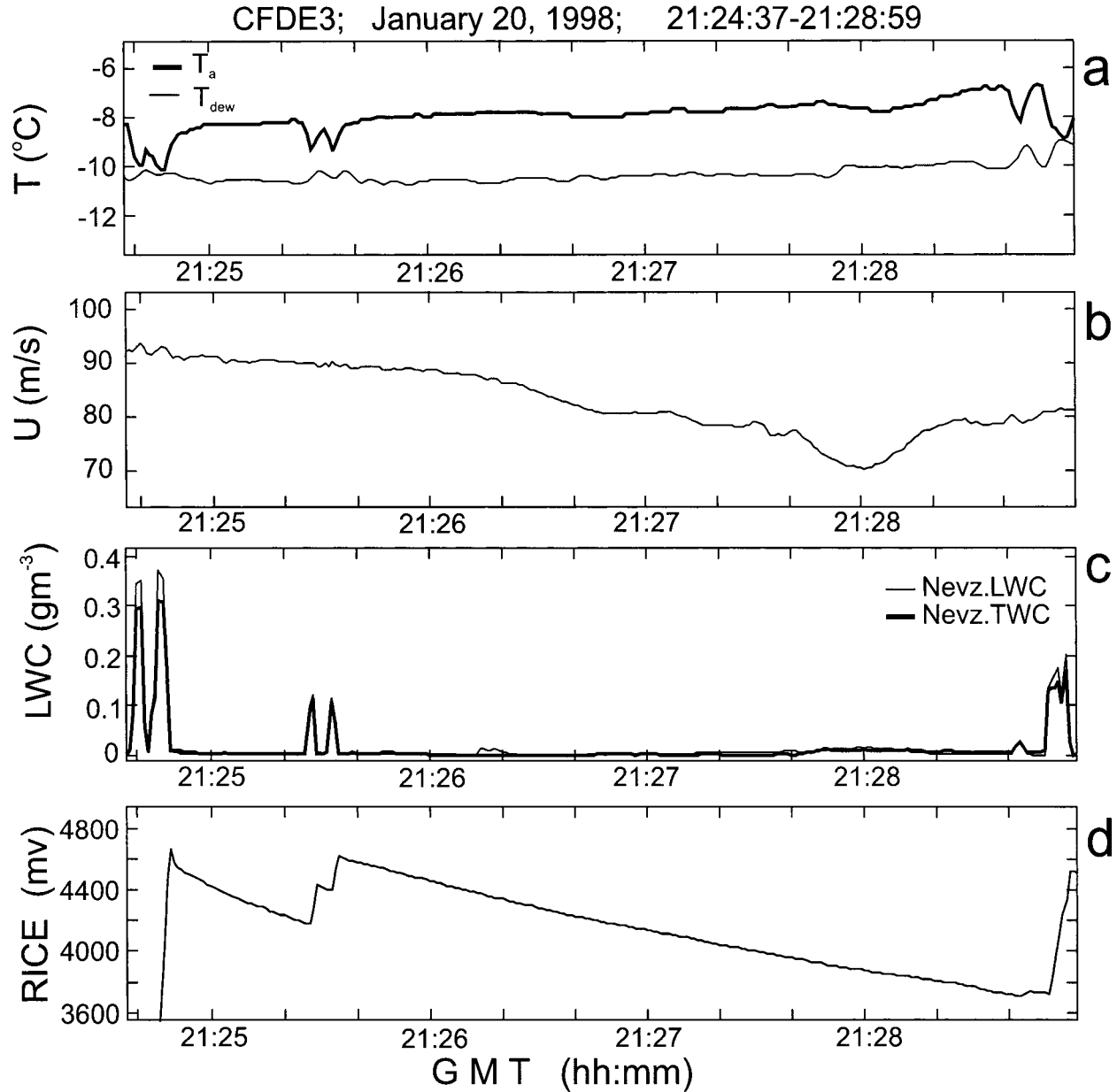


FIG. 6. In situ measurements of (a) air temperature T_a and dewpoint temperature T_{dew} , (b) airspeed U , (c) liquid water content, and (d) RICE signal. The measurements were conducted during Canadian Freezing Drizzle Experiment 3 from NRC Convair-580.

$< 0.1 \text{ g m}^{-3}$ with accuracy $\delta T = 1^\circ\text{C}$, and $\delta W = 0.002 \text{ g m}^{-3}$ 12 iterations are required. The number of iterations increases with an increase in temperature and decrease of the air pressure.

6. RICE probe calibration

The objective of the calibration is to find the coefficient k , which relates the signal V and the mass of the accreted ice M on the RICE probe cylinder [Eq. (1)].

a. "Sublimating" technique

The conventional techniques derive the coefficient k for the cases when ice is growing on the cylinder, that is, $dM/dt > 0$ (Baumgardner and Rodi 1989; Heymsfield and Miloshevich 1989; Claffey et al. 1995). However, Eq. (1) does not imply any limitations on the sign of dM/dt . Therefore, there is a possibility to calibrate the RICE by measuring the rate of ice sublimation in cloud-free air. Figure 6 shows an example of the time history of the RICE probe signal during ice accretion inside

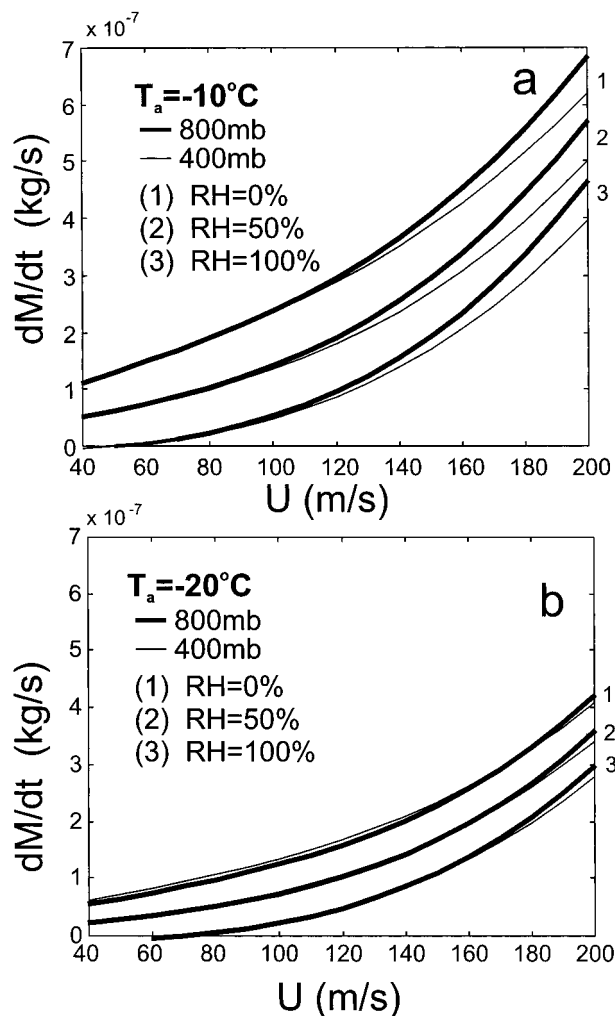


FIG. 7. The rate of ice sublimation from the RICE sensor dM/dt vs airspeed U for different pressure P_a , temperature T_a , and relative humidity RH.

clouds and sublimation in the cloud-free regions. After leaving cloud (Fig. 6c), ice retained on the RICE probe started to sublimate in cloud-free air resulting in a decrease in the RICE probe signal (Fig. 6d). The measured rate of the RICE probe signal reduction $\Delta V/\Delta t$ and the rate of ice sublimation calculated theoretically based on the measurements of U , T_a , P_a , e_a can be used for calibration of the probe.

Figure 7 shows the rate of ice sublimation derived from Eqs. (16) and (19) for the assumption $W = 0$. The rate of sublimation increases rapidly with an increase of the airspeed and decrease of the humidity. For example, at $T_a = -20^\circ\text{C}$ and $e_a = E_w$ the rate of ice sublimation at $U = 200 \text{ m s}^{-1}$ is approximately 14 times larger than that at $U = 100 \text{ m s}^{-1}$. This illustrates how significant ice sublimation can be for high-speed airplanes. It is worth mentioning that ice may grow up on the cylinder at low airspeeds even when flying in cloud-free air. Thus, at temperature $T_a = -20^\circ\text{C}$ and $e_a = E_w$

the ice starts to build up at $U < 60 \text{ m s}^{-1}$ (Fig. 7b). It happens when the vapor pressure in the air becomes larger than the saturation pressure over ice at the surface temperature.

The coefficient k is related to the rate of ice evaporation M_e as

$$k = -\frac{M_e \Delta t}{\Delta V}. \quad (25)$$

Substituting Eq. (20) into Eq. (25) yields

$$k = -\frac{2R_c l \varepsilon U W_e \Delta t}{\Delta V} = -\frac{2R_c l R_a \varepsilon \varphi_0 \xi \alpha \Delta t}{P_a R_v \Delta V} (E_i - e_a). \quad (26)$$

The advantage of this technique is that it derives the coefficient k from first principles and does not need reference measurements of liquid water content.

For calibration purposes, a flight leg should be chosen in cloud-free air where the pressure, air temperature, humidity, and airspeed stay approximately constant. Measuring the signal changes ΔV during time Δt and substituting into Eq. (26) gives the calibrating coefficient k . The vapor pressure E_s is calculated using the temperature T_s , whereas the temperature T_s is calculated from Eq. (16) using in situ measurements of U , T_a , P_a , e_a , and assuming $W = 0$.

Figure 8 presents results of calibrations of three different RICE probes mounted on three different aircraft: Convair-580, King Air, and Sabreliner. In the calculations of k in Eq. (26) it was assumed $l = 2.54 \text{ cm}$, $R_c = 0.317 \text{ cm}$, $\xi = 1.41$, $\varphi_0 = 1.48 \text{ rad}$ (appendix A). The airspeed U , temperature T_a , pressure P_a , and dewpoint temperature T_{dew} were measured by the aircraft instrumentation. Water vapor pressure e_a was calculated from the dewpoint temperature T_{dew} measured by an EG&G dewpoint thermometer. Figure 8a shows the results of calibration of the Meteorological Service of Canada (MSC) RICE probe mounted on the National Research Council (NRC) Convair-580. The measured parameters changed in the ranges $85 \text{ m s}^{-1} < U < 115 \text{ m s}^{-1}$, $-23^\circ\text{C} < T_a < -7^\circ\text{C}$, $0.46 \text{ mb} < e_a < 2.6 \text{ mb}$, $525 \text{ mb} < P_a < 950 \text{ mb}$. Figure 8b shows the results for the National Center for Atmospheric Research (NCAR) RICE probe installed on the King Air. The measured parameters changed in the ranges $115 \text{ m s}^{-1} < U < 140 \text{ m s}^{-1}$, $-29^\circ\text{C} < T_a < -9^\circ\text{C}$, $0.18 \text{ mb} < e_a < 1.5 \text{ mb}$, $390 \text{ mb} < P_a < 550 \text{ mb}$. Figure 8c shows the results for another RICE probe installed on the NCAR Sabreliner. The measured parameters changed in the ranges $U = 180 \text{ m s}^{-1}$, $-34^\circ\text{C} < T_a < -30^\circ\text{C}$, $0.07 \text{ mb} < e_a < 0.18 \text{ mb}$, $365 \text{ mb} < P_a < 375 \text{ mb}$.

The RICE coefficients k are found to be noticeably different and equal to $1.40 \times 10^{-5} \pm 0.14 \times 10^{-5} \text{ kg V}^{-1}$ (MSC Fig. 8a); $2.13 \times 10^{-5} \pm 0.39 \times 10^{-5} \text{ kg V}^{-1}$ (NCAR Fig. 8b); $3.49 \times 10^{-5} \pm 0.41 \times 10^{-5} \text{ kg V}^{-1}$ (NCAR Fig. 8c). This result is consistent with the study of Baumgardner and Rodi (1989) who stated that the coefficient k may be significantly different from probe

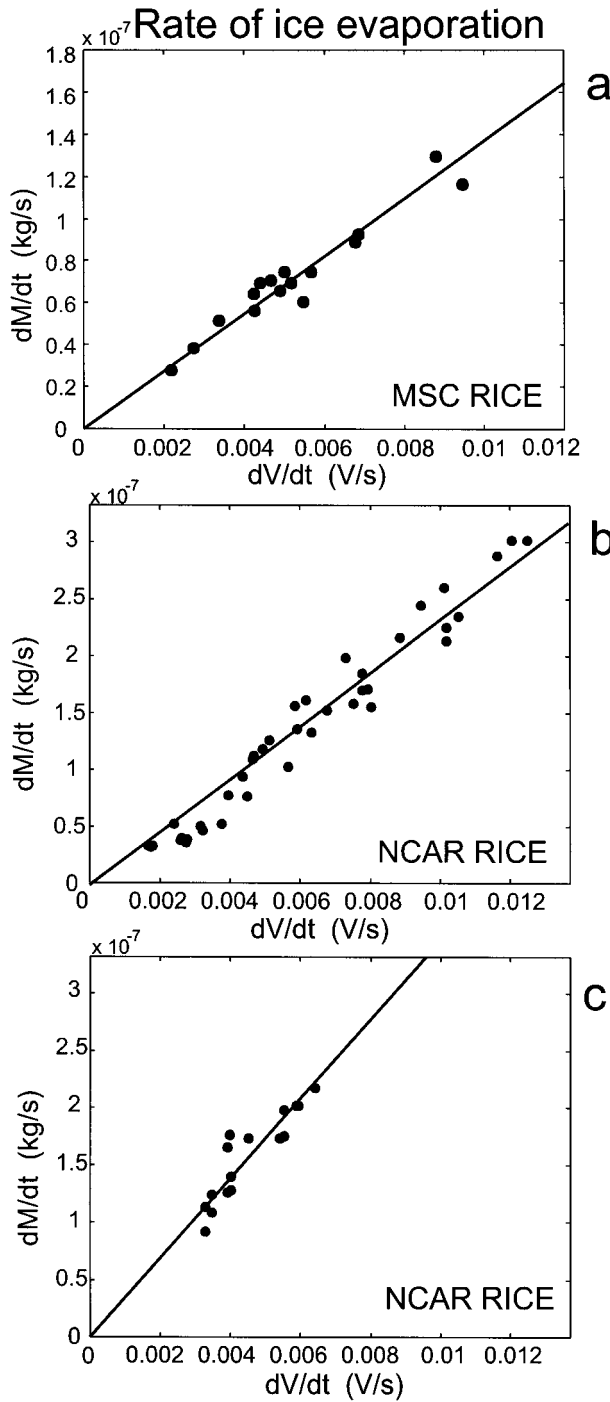


FIG. 8. Calibration of three different RICE probes using the sublimating method: (a) MSC, Convair-580, $k = 1.40 \times 10^{-5} \pm 0.14 \times 10^{-5} \text{ kg V}^{-1}$; (b) NCAR, King Air, $k = 2.13 \times 10^{-5} \pm 0.39 \times 10^{-5} \text{ kg V}^{-1}$; (c) NCAR, Sabreliner, $k = 3.49 \times 10^{-5} \pm 0.41 \times 10^{-5} \text{ kg V}^{-1}$.

to probe. Another explanation may be related to the effect of the RICE probe installation location on the aircraft. If the cylinder is mounted too close to the fuselage or the wing surface, it may cause nonuniform

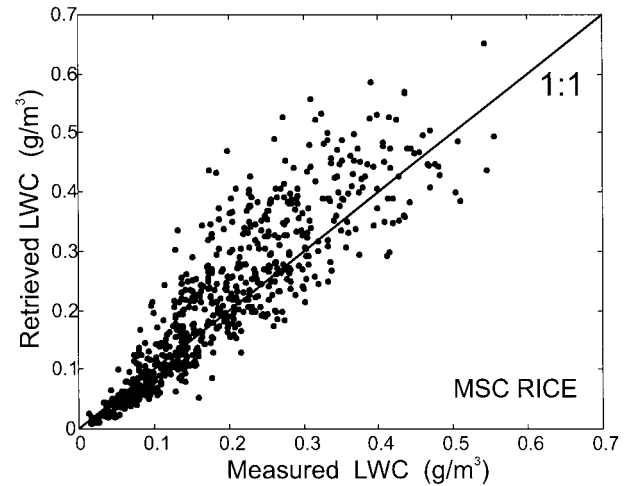


FIG. 9. LWC retrieved from RICE measurements (W_r) vs measured LWC (W_m): W_r was retrieved using the coefficient k derived from the sublimating technique, and W_m was measured by the hot-wire Nevzorov probe (see text).

deposition of ice on the cylinder due to the gradient of the airspeed in the vicinity of the airplane surface. This may result in different length l of the ice deposition along the cylinder's axis, so that the length l may not necessarily be equal to the length of the cylinder. The errors related to changes of local temperature and, consequently, E_s are relatively small and cannot explain the observed difference in k (see sections 4 and 8).

b. Retrieval of liquid water content

The adequacy of the proposed method was tested by a comparison of LWC measured from other probes (W_m) with the LWC retrieved from RICE measurements (W_r) using calibrating coefficient k derived from the “sublimation” technique.

Figure 9 shows a scatterplot of W_m versus W_r . The measurements of LWC W_m were conducted with the help of the airborne hot-wire Nevzorov probe (Korolev et al. 1998) installed in the NRC Convair-580. The accuracy of the Nevzorov probe in measurements of cloud LWC is estimated as 10%. The data were collected mainly in stratiform clouds associated with frontal systems during the Third Canadian Freezing Drizzle Experiment (Isaac et al. 1998) in December 1997–February 1998.

The retrieved liquid water content W_r was calculated as

$$W_r = k \frac{\Delta V}{\Delta t}, \tag{27}$$

where ΔV is the RICE probe signal change during time Δt . The time period Δt for each measurement was taken after the temperature of the cylinder cools down to the air temperature. This was done to avoid the effect of the cylinder residual overheating after a de-icing cycle (Baumgardner and Rodi 1989). The time periods Δt were selected manually for each RICE probe icing cycle

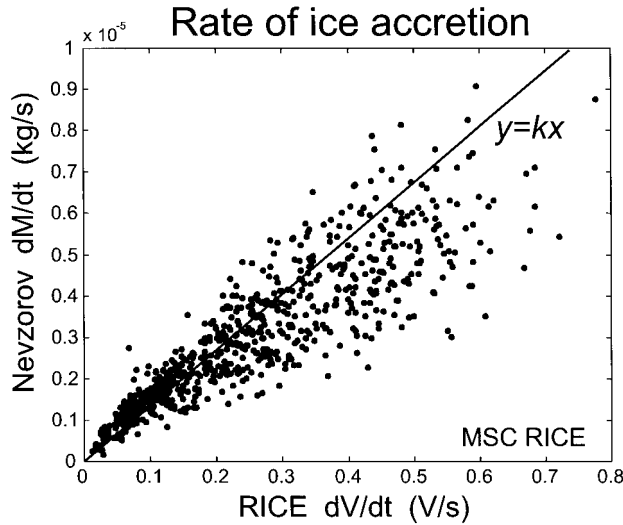


FIG. 10. Calibration of the MSC RICE probe using the ice accretion technique. Here dM/dt was measured by the Nevzorov probe, dV/dt was derived from the RICE probe measurements, and $k = 1.35 \times 10^{-5} \pm 0.42 \times 10^{-5} \text{ kg V}^{-1}$.

and they varied from 2 to 75 s. The measured LWC W_m shown in Fig. 9 was averaged over a time period Δt . Figure 9 shows over 710 different triggering cycles of the RICE probe at temperatures $-6^\circ\text{C} < T_a < -23^\circ\text{C}$, airspeeds $80 \text{ m s}^{-1} < U < 130 \text{ m s}^{-1}$, and pressures $400 \text{ mb} < P < 900 \text{ mb}$, representing a dataset that covers a large variety of cloud situations. Figure 9 indicates that on average W_r and W_m are in good agreement, though the scatter is relatively high. The average ratio of the measured and retrieved LWC $W_r/W_m = 1.11 \pm 0.35$, and the correlation coefficient is 0.85. This comparison supports the “sublimating” technique for the RICE probe calibration.

c. “Ice accretion” technique

The coefficient k obtained for the MSC RICE probe using the “sublimating” technique was compared to that calculated using the conventional technique, that is, when the ice was growing up on the cylinder’s surface. The coefficient k has been calculated as

$$k = 2R_c l \varepsilon U (W_m - W_e) \frac{\Delta t}{\Delta V} \cong 2R_c l U W_m \frac{\Delta t}{\Delta V}. \quad (28)$$

Here it was assumed that the collection efficiency is $\varepsilon = 1$ for both the RICE probe and Nevzorov probes.

Figure 10 shows the scatterplot of the rate of ice accretion $dM/dt = 2R_c l U \overline{W}_m$, calculated from in situ measurements of U and \overline{W}_m versus the rate of the RICE probe signal changes $\Delta V/\Delta t$. Here \overline{W}_m is measured LWC averaged over time Δt .

The average value of the coefficient calculated for the dataset shown in Fig. 10 is $k = 1.35 \times 10^{-5} \pm 0.42 \times 10^{-5} \text{ kg V}^{-1}$, and the correlation coefficient is 0.88.

The value of k calculated using the ice accretion technique is rather close to that obtained using the sublimating technique $1.40 \times 10^{-5} \pm 0.14 \times 10^{-5} \text{ kg V}^{-1}$, though the dispersion is three times higher.

7. Discussion

a. Accuracy of the sublimating technique

The accuracy of the RICE probe calibration using the “sublimating” technique depends on the accuracy of measurements of U , T_a , P_a , T_{dew} , and assumptions about R_c , l , ε , φ_0 , α , and ξ . The first four measurable parameters result in random errors and are mainly responsible for the scatter in Fig. 8. The remaining parameters would result in systematic errors. The angle φ_0 is defined by Re and Stk numbers and it increases approaching $\pi/2$ with an increase of droplet size. During sublimation, the angle φ_0 decreases as well as the length l and the radius R_c of the iced cylinder. During aircraft measurements, it is not possible to control R_c , l , or φ_0 . For the calculations presented in Fig. 8 the following assumptions regarding R_c , l , φ_0 , ε , and ξ were made.

- 1) The length of ice is equal to the length of the RICE probe cylinder, that is, $l = 2.54 \text{ cm}$.
- 2) The radius of curvature of the ice is equal to the cylinders radius $R_c = 0.317 \text{ cm}$.
- 3) The collision efficiency ε was calculated based on Re and Stk numbers (appendix B). In the calculation it was assumed that $r = 10 \mu\text{m}$. For most cases ε was no less than 0.9.
- 4) The angle is equal to $\varphi_0 = 1.48 \text{ rad}$ for $\varepsilon = 0.9$. Angle φ_0 is a function of Re and Stk.
- 5) The coefficient $\xi = 1.41$ for the angle $\varphi_0 = 1.48$ (appendix A).

Differentiating the logarithm of Eq. (26) yields an equation for estimating the effect of errors on the accuracy of calculation of k :

$$\frac{\delta k}{k} = \frac{\delta R_c l}{R_c l} + \frac{\delta \varepsilon \varphi_0}{\varepsilon \varphi_0} + \frac{\delta \xi \alpha}{\xi \alpha} + \frac{\delta(E_{is} - e_a)}{E_{is} - e_a} - \frac{\delta P_a}{P_a}. \quad (29)$$

During ice sublimation, φ_0 and l decrease, whereas ξ and E_i increase. The net effect of the ice sublimation results in a decrease of the product $R_c l \varphi_0 \xi (E_{is} - e_a)$. For calibration purposes, the vague $\Delta V/\Delta t$ should be measured at the beginning of sublimation, before φ_0 , l , and R_c start to change.

A variation of r within $2 \mu\text{m}$ results in errors $\xi \varphi_0$ within 3%–5%. The value of $\xi \alpha$ changes no more than 5%. The relative effect of uncertainty in $R_c l$ is estimated as 3%–5%. The air pressure P can be measured with high accuracy so that the relative errors due to P are less than 1%. The errors of 1°C in measurement of T_a and T_{dew} can result in relative errors in the term $(E_{is} - e_a)$ of 10%–20%. The relative error in measurements $(E_{is} - e_a)$ may increase when e_a is close to saturation.

The net effect of all errors may reach easily 20%–30%, which explains the scatter in diagrams in Fig. 8.

b. Accuracy of ice accretion technique

The accuracy of the RICE probe calibration using the rate of the ice growth on the cylinder depends significantly on the accuracy of the measurement of LWC by a reference probe. Usually, either the FSSP or hot-wire probes such as the King or Nevzorov probes are used as a reference. In the best case for the hot-wire probes the accuracy of the measurements of LWC is about 10%–15%. For LWC derived from FSSP measurements the errors may be up to 30% or more for liquid water clouds. For mixed clouds the FSSP measurements may be “contaminated” by ice particles and that may result in much higher errors. The net effect of uncertainties in R_c , l , and ε may result in errors about 20%. The measurements of true airspeed are rather accurate compared to other sources of errors and therefore they can be neglected. The resulting accuracy of the conventional RICE probe calibrating technique is estimated as 25%–30%.

However, the above estimate does not explain the scatter of the data in Figs. 9 and 10 where the retrieved and measured LWC may be different by a factor of 2. An additional source of error may be related to the changes of the airflow around the cylinder due to different aircraft maneuvers, such as changes of the angle of attack, climbs, descents, turns, etc. These may affect the local airflow around the cylinder or result in partial aerodynamic shadowing of the cylinder.

It should be noted that the RICE probe has a significant “dead” (or “delay”) time compared to other probes used for the measurements of LWC. During this time period the cylinder is heated to de-ice its surface and then it cools down to the air temperature. The heat balance on the surface of the icing cylinder cannot be considered as a steady state during the dead time, and the theoretical consideration developed above is not applicable for these conditions. Such periods must be excluded from measurements of $\Delta V/\Delta t$. Dead time is a function of W , T_a , P_a , U , and it may vary from 10% to 90% of the measurement cycle. The fraction of the dead time increases with an increase in U and W and decrease of T_a . Similar results were found by Baumgardner and Rodi (1989).

c. Measurements in mixed and glaciated clouds

Though the RICE probe shows relatively large scatter in measurements of LWC (Figs. 8, 9), it can be effectively used in studies of mixed and glaciated clouds. For now it is the only known aircraft instrument used in cloud physics measurements that responds to the liquid phase and is insensitive to ice particles. It should be emphasized that the imaging probes, such as PMS OAPs or CPI, do not provide phase recognition for cir-

cular particles, since frozen droplets would appear in 2D imagery in the same way as liquid ones. At the same time the hot-wire probes like the King or Nevzorov probes may have a residual effect of ice particles on measurements (Korolev et al. 1998). The following example demonstrates the capability of the RICE probe in mixed and glaciated environment. Figure 11 shows synchronous measurements of the RICE probe signal and LWC derived from FSSP data. The measurements were conducted by NCAR Sabreliner in wave clouds in 1990 (Heymsfield and Miloshevich 1993). It is clearly seen that the RICE probe repeatedly triggers in approximately half of each cloud during the penetration through it. These triggers are caused by the portion of cloud containing some liquid. In the other parts of the clouds the RICE signal is decreasing due to ice sublimation, which indicates zero LWC and, consequently, complete glaciation of the cloud. This example also demonstrates that FSSP may give rather erroneous measurements of *liquid* water content in cold clouds. This would create problems in calibrating the RICE probe using the FSSP measurements of LWC.

8. Conclusions

The above study results in the following conclusions.

- 1) Theoretical examination of the rate of ice accretion on the RICE probe cylinder showed that the minimum measured liquid water is limited by the lower threshold W_{e0} [Eq. (20)]. A liquid water less than W_{e0} cannot be detected by the RICE probe. The value of W_{e0} is mainly defined by T_a , and U . For high airspeeds ($U > 200 \text{ m s}^{-1}$) the threshold value W_{e0} may well exceed 0.01 g m^{-3} , which may become comparable with the measured cloud liquid water content.
- 2) The upper limit of the measured LWC by the RICE probe is determined by the Ludlam limit W_{cr} [Eq. (22)]. The value of W_{cr} depends on P , T_a , and U . For typical aircraft speeds ($80 \text{ m s}^{-1} < U < 200 \text{ m s}^{-1}$) in the temperature range $-5^\circ\text{C} < T_a < -15^\circ\text{C}$ the Ludlam limit for the RICE probe ranges from 0 to 0.8 g m^{-3} (Fig. 5) and such conditions can be easily met in clouds. If the liquid water content exceeds W_{cr} the RICE probe cannot be used for accurate measurements of LWC.
- 3) A new technique for the calibration of the RICE probe based on the measurements of the rate of ice sublimation in cloud-free air is proposed. The advantage of the method is that it derives the calibration coefficient from first principles and it does not require reference measurement of LWC by other probes. The conventional RICE probe calibration technique is based on the measurement of the rate of ice growth and it needs in addition measurements of LWC. The comparative analysis in section 7c showed that the accuracy of the sublimating cali-

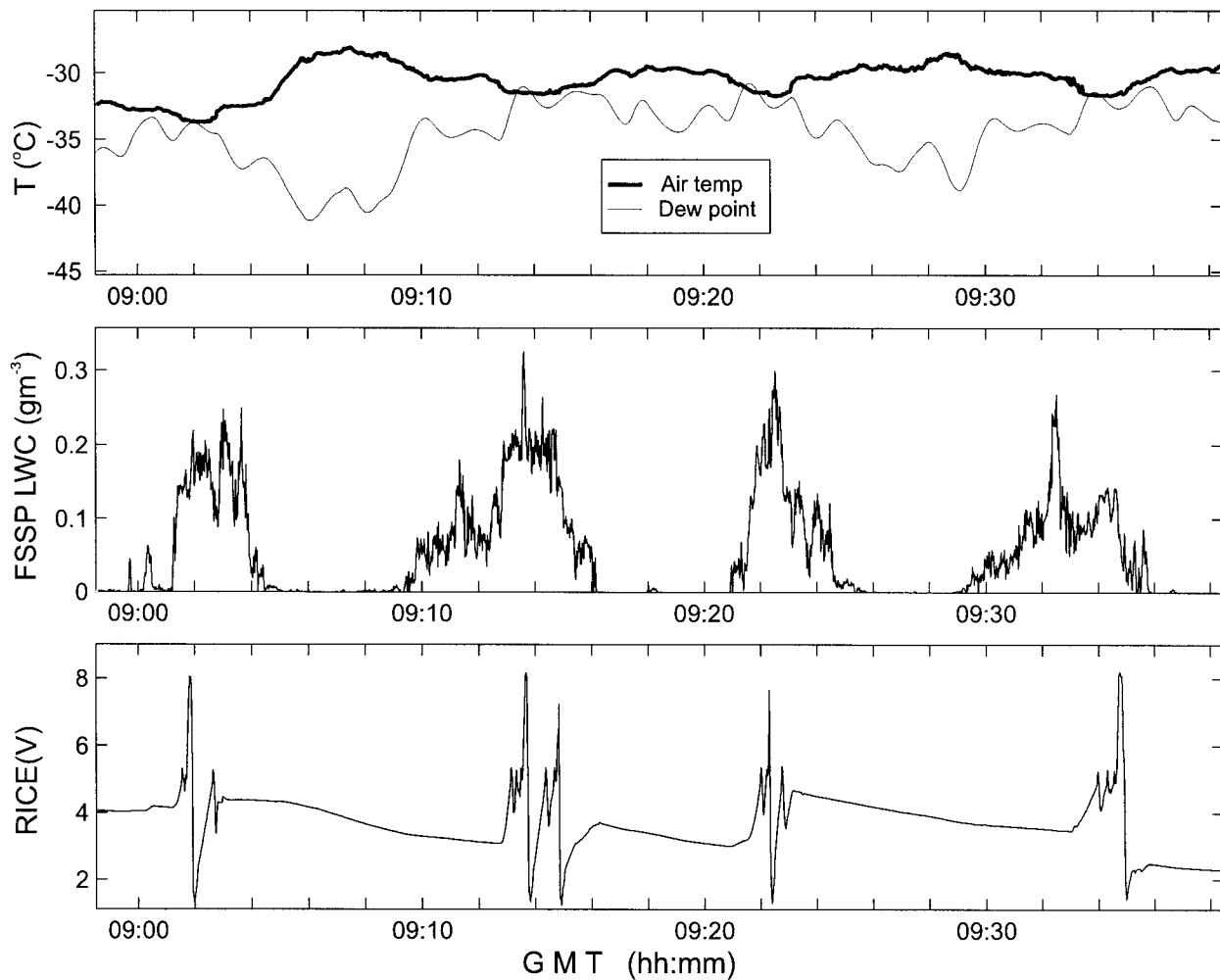


FIG. 11. Time history of (a) air and dewpoint temperature, (b) LWC calculated from FSSP measurements, and (c) RICE signal. The measurements were conducted by the NCAR King Air in 1990 in wave clouds.

bration technique is better compared to the conventional ice accretion technique.

The range of possible supercooled LWCs measured by the RICE probe is limited by W_{e0} and W_{cr} . Since W_{e0} increases and W_{cr} decreases with an increase of the airspeed U , the range of measured LWC decreases with the increase of U . Therefore, the use of the RICE probe for measurements of supercooled LWC from slow moving platforms would be more effective compared to high-speed ones. For example at $U > 200 \text{ m s}^{-1}$, $T_a > -10^\circ\text{C}$, and $P > 800 \text{ mb}$ the RICE probe cannot be used for proper measurements of LWC since $W_{cr} = 0$ (Fig. 5). Though the RICE probe will trigger under these conditions due to partial freezing of water on the upwind surface of the cylinder and runback icing. The use of the RICE at low airspeeds is also preferable because of a smaller fraction of the dead time compared to high speed under the same conditions.

Low accuracy, large dead times, and complex data

postprocessing may significantly limit the capability of RICE probe for measurements of supercooled cloud liquid water. That is why in aircraft cloud microphysics studies the RICE probe is mainly used as a detector of supercooled liquid water. This is one of the most advantageous properties of the RICE probe, since the phase discriminating capability of hot-wire probes are limited due to the residual effect of ice particles (Korolev et al. 1998) and FSSP does not provide reliable LWC measurements in mixed-phase conditions. Nevertheless the RICE probe could be used as a useful additional tool for estimation of LWC values.

Acknowledgments. The authors would like to thank the financial support of the Canadian National Search and Rescue Secretariat and Transport Canada. In addition, we are grateful for the support from colleagues at the National Research Council of Canada and others at the Meteorological Service of Canada. Special thanks

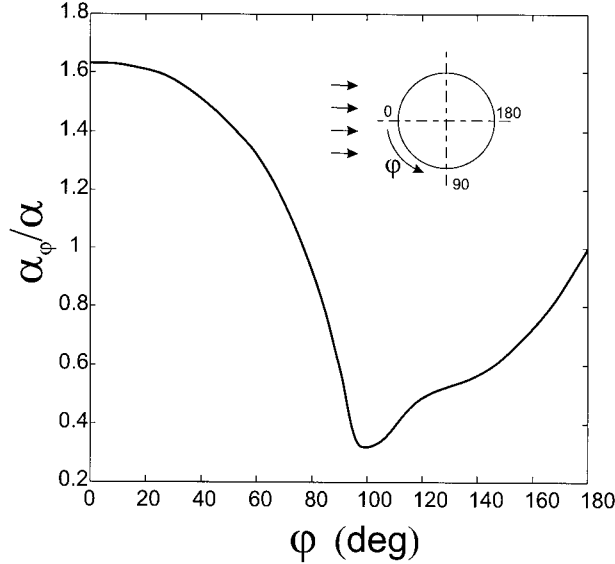


FIG. A1. Relative heat transfer coefficient for a circular cylinder $\alpha_\varphi/\bar{\alpha}$ vs angle φ along the circumference.

for Dave Rogers and two anonymous reviewers for valuable comments that certainly helped to improve the manuscript.

APPENDIX A

Heat Transfer Coefficient

The heat transfer coefficient in a local point on the surface of the cylinder α_φ is a function of the polar angle φ . Figure A1 shows the dependence of α_φ/α versus φ (Mikheev 1949), here α is the heat transfer coefficient averaged over the whole cylinder, that is, $-\pi < \varphi < \pi$. The average value of the heat transfer coefficient α can be expressed in terms of the Nusselt number

$$\text{Nu} = \frac{2\alpha R_c}{\lambda}, \quad (\text{A1})$$

where λ is thermal conductivity of air. For the flow around circular cylinder the Nusselt number is related to the Reynolds number as (e.g., Mikheev 1949; Kreith and Bohn 1986)

$$\text{Nu} = A\text{Re}^n. \quad (\text{A2})$$

Substituting Eq. (A1) in Eq. (A2) yields

$$\alpha = \frac{A\lambda}{2R_c} \left(\frac{2UR_c}{\nu} \right)^n. \quad (\text{A3})$$

Here ν is kinematic viscosity. Due to Mikheev (1949) for $\text{Re} > 5 \times 10^3$ the coefficients $A = 0.197$ and $n = 0.6$. For the RICE probe $\text{Re} > 5 \times 10^3$ corresponds to the airspeeds $U > 10 \text{ m s}^{-1}$ at $P_a = 1000 \text{ mb}$ and $T_a = 0^\circ\text{C}$. Therefore, the values of coefficients a and n are applicable for the following calculations.

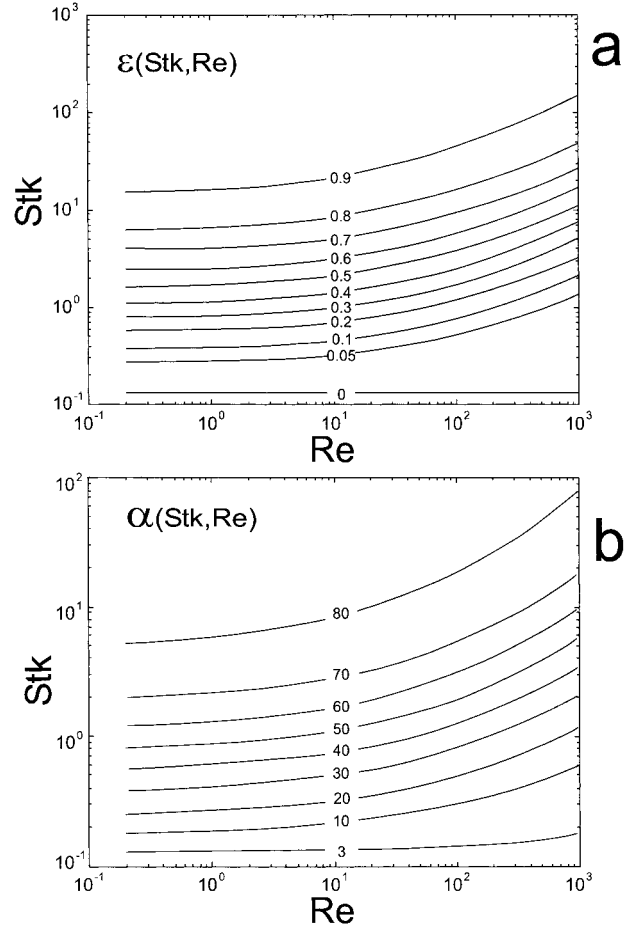


FIG. B1. Dependence of (a) collision efficiency ε and (b) polar angle φ for circular cylinder vs Re and Stk numbers.

The average heat transfer coefficient $\bar{\alpha}_\varphi$ for the range of angles $-\varphi$ to φ can be found as

$$\bar{\alpha}_\varphi = \xi\alpha. \quad (\text{A4})$$

The coefficient ξ can be obtained by integrating the curve in Fig. A1 for the angle range 0 to φ . For $\varphi = 1.48 \text{ rad}$ the integrating results in $\xi = 1.41$.

APPENDIX B

Collision Efficiency

The ratio of the distance between glancing droplet trajectories hitting the cylinder in undisturbed air to the cross-section of a body is called the total collision efficiency ε . The collision efficiency for cylinder is a function of Stokes $\text{Stk} = (2Ur^2)/(9\mu R_c)\rho_w$ and Reynolds $\text{Re} = (2Ur)/\nu$ numbers, where R_c is the radius of cylinder; μ and ν are the dynamic and kinematic viscosity, respectively; and ρ_w is the water density. Figure B1a shows the diagram of ε isolines in the Re – Stk coordinates calculated from Langmuir and Blodgett (1945), based on solution of equation of droplet motion in the

air flowing around the circular cylinder (Mazin 1957). The polar angle φ defines the sector within which the droplets impact with the cylinder. At angles larger $|\varphi|$ droplets do not hit the surface of the cylinder and flow away with the air. The angle φ is a function of Re and Stk numbers. Figure B1b show the isolines of φ in the Re–Stk coordinates (Mazin 1957). The diagrams in Fig. B1 were used for calculation φ and ε . For example, for $U = 100 \text{ m s}^{-1}$, $r = 7 \text{ }\mu\text{m}$, $T_a = -20^\circ\text{C}$, $P_a = 600 \text{ mb}$, we find $\text{Stk} \cong 21$, $\text{Re} \cong 72$, $\varepsilon \cong 0.84$, $\varphi = 82^\circ$. For $U = 100 \text{ m s}^{-1}$, $r_3 = 10 \text{ }\mu\text{m}$, $T_a = -10^\circ\text{C}$, $P_a = 800 \text{ mb}$, and $\text{Stk} \cong 42$, $\text{Re} \cong 130$, $\varepsilon \cong 0.88$, and $\varphi_0 = 84^\circ$.

REFERENCES

- Baumgardner, D., and A. Rodi, 1989: Laboratory and wind tunnel evaluation of the Rosemount icing detector. *J. Atmos. Oceanic Technol.*, **6**, 971–979.
- Borovikov, A. M., I. I. Gaivoronskii, E. G. Zak, V. V. Kostarev, I. P. Mazin, V. E. Minervin, A. Kh. Khrgian, and S. M. Shmeter, 1963: *Cloud Physics*. Israel Program of Scientific Translations, 393 pp.
- Brown, E. N., 1982: Ice detector evaluation for aircraft hazard warning and undercooled water content measurements. *J. Aircraft*, **19**, 980–983.
- Claffey, K. J., K. F. Jones, and C. C. Ryerson, 1995: Use and calibration of Rosemount ice detectors for meteorological research. *Atmos. Res.*, **36**, 277–286.
- Cober, S. G., G. A. Isaac, and A. V. Korolev, 2000: Assessing the Rosemount Icing Detector with in-situ measurements. *J. Atmos. Oceanic Technol.*, **18**, 515–528.
- Fraser, D., C. K. Rush, and D. Boxter, 1953: Thermodynamic limitations of ice accretion instruments. *Bull. Amer. Meteor. Soc.*, **34**, 146–154.
- Greenan, B. J., and R. List, 1995: Experimental closure of the heat and mass transfer theory of spheroidal hailstones. *J. Atmos. Sci.*, **52**, 3797–3815.
- Hardy, J. K., 1945: Kinetic temperature of wet surfaces, a method of calculating the amount of alcohol required to prevent ice, and the derivation of the psychrometric equation. *N.A.C. A. ARR*, **5013**, 13 pp.
- , and C. D. Brown, 1954: Kinetic temperature of propeller blades in conditions of icing. Aeronautical Research Council Reports and Memo., Rep. 2806, 12 pp.
- Heymtsfield, A., and L. Miloshevich, 1989: Evaluation of liquid water measuring instruments in cold clouds sampled during FIRE. *J. Atmos. Oceanic Technol.*, **6**, 378–388.
- , and —, 1993: Homogeneous ice nucleation and supercooled liquid water in orographic wave clouds. *J. Atmos. Sci.*, **50**, 2335–2353.
- Hilton, W. F. 1951: *High-Speed Aerodynamics*. Longmans, Green, 598 pp.
- Incropera, F. P., and D. P. DeWitt, 1985: *Fundamental of Heat and Mass Transfer*. Wiley, 802 pp.
- Isaac, G. A., S. G. Cober, A. V. Korolev, J. W. Strapp, A. Tremblay, and D. L. Marcotte, 1998: Overview of the Canadian Freezing Drizzle Experiment I, II, and III. Preprints, *14th Conf. on Cloud Physics*, Everett, WA, Amer. Meteor. Soc., 447–450.
- Korolev, A. V., J. W. Strapp, G. A. Isaac, and A. N. Nevzorov, 1998: The Nevzorov airborne hot-wire LWC-TWC probe: Principle of operation and performance characteristics. *J. Atmos. Oceanic Technol.*, **15**, 1495–1510.
- Kreith, F., and M. S. Bohn, 1986: *Principles of Heat Transfer*. Harper and Row Publishers, 700 pp.
- Langmuir, I., and K. Blodgett, 1945: A mathematical investigation of water droplet trajectories. *Collected Works of I. Langmuir*, Vol. 10, Pergamon Press, 348–393.
- Lozowski, E. P., and J. R. d'Amours, 1980: A time-dependent numerical model for spherically symmetric hailstone growth thermodynamics under constant ambient conditions. *J. Atmos. Sci.*, **37**, 1808–1820.
- , J. R. Stallabrass, and P. F. Hearty, 1983a: The icing of an unheated, nonrotating cylinder. Part I: Simulation model. *J. Climate Appl. Meteor.*, **22**, 2053–2062.
- , —, and —, 1983b: The icing of an unheated, nonrotating cylinder. Part II: Icing wind tunnel experiment. *J. Climate Appl. Meteor.*, **22**, 2063–2074.
- Ludlam, F. N., 1951: The heat economy of rimed cylinder. *Quart. J. Roy. Meteor. Soc.*, **77**, 663–666.
- Makkonen, L., 1981: Estimating intensity of atmospheric ice accretion on stationary structures. *J. Appl. Meteor.*, **20**, 595–600.
- Mazin, I. P., 1957: *The Physical Principles of Aircraft Icing* (in Russian). Gidrometeoizdat, 120 pp.
- Messinger, B. L., 1953: Equilibrium temperature of an unheated surface as a function of airspeed. *J. Aeronaut. Sci.*, **20**, 29–41.
- Mikheev, M. A., 1949: *Principles of Heat Transmission* (in Russian). Gosenergoizdat, 396 pp.
- Minervin, V. E., 1956: About measurements of liquid water content and icing in supercooled liquid clouds and some errors of measurements (in Russian). *Trudi TsAO*, **17**, 15–35.
- Seban, R. A., 1960: The influence of free stream turbulence on the local heat transfer from cylinder. *J. Heat Transfer*, **82**, 101–107.
- Tribus, M., 1951: Intermittent heating for protection in aircraft icing. *Trans. ASME*, **73**, 83 pp.